

# Spatial distribution of average charge state and deposition rate in high power impulse magnetron sputtering of copper

David Horwat<sup>1,2,\*</sup> and André Anders<sup>1</sup>

<sup>1</sup> Lawrence Berkeley National Laboratory, University of California, 1 Cyclotron Road, Berkeley, California 94720, USA

<sup>2</sup> Laboratoire de Science et Génie des Surfaces, Nancy-Université, CNRS, Parc de Saurupt CS 14234 F-54042 Nancy, France

\* corresponding author, e-mail: [David.Horwat@mines.inpl-nancy.fr](mailto:David.Horwat@mines.inpl-nancy.fr)

## Abstract

The spatial distribution of copper ions and atoms in high power impulse magnetron sputtering (HIPIMS) discharges was determined by (i) measuring the ion current to electrostatic probes and (ii) measuring the film thickness by profilometry. A set of electrostatic and collection probes were placed at different angular positions and distances from the target surface. The angular distribution of the deposition rate and the average charge state of the copper species (including ions and neutrals) were deduced.

The discharge showed a distinct transition to a high current mode dominated by copper self-sputtering when the applied voltage exceeded the threshold of 535 V. For a lower voltage, the deposition rate was very low and the average charge state was found to be less than 0.4. For higher voltage (and average power), the absolute deposition rates were much higher, but they were smaller than the corresponding direct current (DC) rates if normalized to the same average power. At the high voltage level, the spatial distribution of the average charge state showed some similarities with the distribution of the magnetic field, suggesting that the generation and motion of copper ions is affected by magnetized electrons. At higher

voltage, the average charge state increases with the distance from the target and locally may exceed unity, indicating the presence of significant amounts of doubly charged copper ions.

Keywords: High power impulse magnetron sputtering, deposition rate, spatial distribution, plasma, average charge state

## 1. Introduction

High Power Impulse Magnetron Sputtering (HIPIMS) is an emerging Physical Vapour Deposition (PVD) technology [1-6]. While conventional magnetron sputtering discharges are characterized by a very low ionisation coefficient of the sputtered species, typically about 0.01 or lower, the ionization of sputtered atoms can occur to much greater extent in HIPIMS discharges [3, 7, 8]. The specific features depend on the characteristics of the discharge and on the sputtered material, and specifically on the high power density dissipated at and near the target surface, the working pressure, the self-sputtering ( $\gamma_{SS}$ ) and secondary electrons emission ( $\gamma_{SE}$ ) yields of the target material [9, 10].

Further deployment of HIPIMS will depend on an improved understanding of the physics of the discharge and the control of reproducible film properties on large surface areas. Another important issue is the somewhat controversial issue of low HIPIMS deposition rates when compared to conventional sputtering rates [5, 11, 12].

We are still in the early stages of the HIPIMS era, when the physics and technology are developed. Indeed, there is still a need to better measure, model, and understand the basic processes. In the present paper we report on the spatial development of a copper HIPIMS discharge with emphasis on the angular distributions of the deposition rate and average copper charge state. To do this, we determine the ion flux and the neutral flux to a set of strategically positioned probes. The ion flux will be measured by the ion saturation current and the combined ion and neutral flux via thickness measurements corrected for resputtering. The results are discussed in relation to the magnetic configuration, secondary emission of electrons and discharge voltage (and corresponding power).

## 2. Experimental

The experiments were carried out using a 2-inch (5 cm) planar, slightly unbalanced magnetron placed horizontally in a 200 litres sputtering chamber. The target was  $\frac{1}{4}$  inch (6.25 mm) thick copper disk. The diameter of the circular racetrack was 25 mm. We intentionally used such a small magnetron because it allowed us to achieve very high power density. Copper was selected for this study due to the high stability of HIPIMS copper discharges (copper can operate in a pure self-sputtering mode [13]).

The strength of the magnetron's magnetic field was deduced from the local axial and radial components of the magnetic field. These components were measured with a Gauss/Tesla meter (F.W. Bell). The induction at the centre of the target surface was 64 mT.

The power was supplied by a slightly modified SPIK2000A pulse power supply (Melec GmbH) operating in the unipolar negative mode. A great feature of this pulser is the ability to freely select the pulse length at a constant voltage. The short pulse limit is given by the pulser to 5  $\mu$ s, and the long pulse limit by the capacitively stored energy, which practically means several milliseconds. We are especially interested in pulses longer than 100  $\mu$ s because this allows the discharge to fully evolve into the sustained self-sputtering (SSS) phase [9, 10, 12, 14]. We used a pulse length of 400  $\mu$ s and pause time of 19600  $\mu$ s, which corresponds to a pulse repetition frequency of 50 Hz. Pure argon gas was supplied near the target, establishing an operational pressure of 1.8 Pa adjusted to by the specific combination of gas flow rate (up to 100 sccm) and pumping speed (cryogenic pump and adjustable throttle valve). At fully opened valve, the pumping speed was 1500 l/s for air, and the chamber base pressure was about  $10^{-4}$  Pa. The total pressure was monitored by an MKS Baratron<sup>®</sup> gauge.

The discharge current was monitored using a current transformer (Pearson<sup>™</sup> model 301X, 0.01 V/A, 2 MHz bandwidth); and the voltage at the target was measured with a 1000:1 fast voltage divider (Tektronix 6015A, 75 MHz bandwidth). The data were recorded on a digital storage oscilloscope (Tektronix TDS5104B) in sample mode.

Eight electrical probes, each consisting of 0.75-inch (1.91 cm) diameter stainless steel disks, were positioned at 14.5, 18.5 or 22.5 cm off the centre of the target surface and arranged along a quarter circle (see Fig. 1). One probe collects the current on the magnetron axis, and the others are off axis yet facing the centre. The angle between two consecutive trajectories between probe and target centre is  $8^\circ$ . That is, the angular distribution of the current is monitored in the range  $34^\circ$ - $90^\circ$  relative to the target surface for three different distances. To be representative of the magnetron geometry, the results are displayed in the range  $34^\circ$ - $146^\circ$  by assuming symmetry around the magnetron axis. Smaller angles were not considered because the anode ring would interfere with the line-of-sight between probe and target.

The electrical insulation between the probes and their metallic holder was ensured by alumina pieces. Each probe was either at floating potential, or each was biased to -60 V with respect to ground (anode potential) to record the time-dependent ion saturation current. The current collected by each probe was monitored using a set of current transformers (Pearson<sup>TM</sup> model 110, 0.1 V/A, 20 MHz bandwidth), and the data were recorded and stored on a digital storage oscilloscope (Tektronix TDS5104B).

At the centre of each probe, a 3 mm x 3 mm piece of doped (conducting) silicon wafer was placed allowing us to measure the deposition rate  $D_{Cu}$  after deposition using profilometry (Dektak IIA). The thickness was checked by scanning electron microscopy (SEM), which also allowed us to image the cross sectional morphology of the films (Phillips XL30S Field Emission Gun SEM). The density of the films was calculated from their thickness and their mass difference, the latter determined by weighing the samples before and after deposition with a microbalance (accuracy 1  $\mu$ g).

### **3. Results and discussion**

### 3.1 General relationships and data evaluation

The total charge that flowed through one probe of area  $S_{probe} = 2.85 \text{ cm}^2$  can be determined by the measured ion current  $I_i(t)$  integrated over the duration of the pulsed ion flow and multiplied by the number of pulses of the experiment:

$$Q_{total} = N_{pulse} \int_{pulse} I_i(t) dt. \quad (1)$$

The corresponding time-averaged **density of charge flux of ions** to a probe can be obtained by introducing the pulse repetition frequency  $f_{pulse} = 50 \text{ Hz}$ :

$$\langle j_Q \rangle_t = \frac{f_{pulse}}{S_{probe}} \int_{pulse} I_i(t) dt. \quad (2)$$

**Comment [A1]:** That is a very unusual way of saying current density !! The unit is  $\text{A/m}^2$ , therefore I suggest saying « ion current density » and change the symbol

**Comment [L2]:** This expression looks right since we need to express the charge flux density (or density of charge flux ???)

The measured probe current is taken to be equal to the current of arriving ions,  $I_i(t)$ , by assuming that the current of secondary electrons from the probe is negligible. The error introduced by this assumption is less than 5% given the very small yields of secondary electron emission for the given conditions.

The apparent (uncorrected) **flux** of copper particles deposited on the probe can be deduced from the deposition rate  $D_{Cu}$  and the copper molar volume  $V_{Cu} = 7.10 \text{ cm}^3 / \text{mol}$ :

$$\Phi_{Cu,app} = \frac{D_{Cu} N_A}{V_{Cu}}, \quad (3)$$

where  $N_A = 6.022 \times 10^{23} \text{ atoms/mol}$  is Avogadro's number. The deposition rate can be found by measuring the thickness and division by the total time,

$$D_{Cu} = \frac{S_{film}}{t_{total}} = \frac{S_{film} f_{pulse}}{N_{pulse}}. \quad (4)$$

However, we have to take into account that not all copper atoms and ions arriving at the surface will stick or remain there. We can do that by correcting for resputtered material, i.e. for the loss of surface atoms caused by the impact of ions on the probe. The Monte Carlo

**Comment [A3]:** The quantity « flux » is by definition « particles/(area \* time), therefore the word « density » is misleading here

code SRIM 2006 [15] provides a means for the quick determination of the self-sputtering yield, giving  $\gamma_{Cu-Cu} = 0.280$  when taking into account a plasma potential of about +10 V and the applied bias voltage of -60 V. The corrected flux of copper particles is then

$$\Phi_{Cu} = \frac{\Phi_{Cu,app}}{1 + \gamma_{Cu-Cu} \Phi_{Cu,app}}. \quad (5)$$

From this quantity and equation (2) one can determine the average charge of copper particles

$$\bar{Q} = \frac{\Phi_Q}{e \langle j_{Cu} \rangle_t}, \quad (6)$$

where  $e = 1.602 \times 10^{-19}$  As is the elementary charge. It should be stressed that this averaging includes atoms *and* ions, and therefore the values for  $\bar{Q}$  can be smaller than unity, indicating the presence of many neutrals, or larger than unity, indicating the presence of multiply charged ions. We have further assumed that the substrate current is determined by copper ions, i.e., the contribution of argon ions is small. This assumption is reasonable when the discharge has switched into the SSS phase because argon is reduced by rarefaction and then additionally replaced by the large flux of copper. In the following we elaborate on runaway and phasing of the HIPIMS discharge.

Figure 2 shows the time dependence of the discharge current  $I_d$  for two discharge voltages, 520 V and 550 V. The difference between those voltages appears at a first glance not that strong. However, as discussed in previous publications [9, 10, 14], there is a threshold at which the process of self-sputtering runs away. Following the original discussion by Hosokawa and coworkers [16] and a recent extension [14], the threshold is defined when the selfsputtering parameter  $\Pi = \alpha\beta\gamma_{SS}$  reaches unity, where  $\alpha$  is the probability that a sputtered atom is ionised,  $\beta$  is the probability that this ion returns to the target, and  $\gamma_{SS}$  is the previously introduced self-sputtering yield. The two voltages 520 V and 550 V represent the situations below and above this threshold. The actual threshold or transition was found at

**Comment [A4]:** I corrected to use « current density » as per updated equation (2)

**Comment [L5]:** Now that looks correct, right ?

about 535 V. Beyond the threshold, the discharge is dominated by metal ions as is evident from many indicators, such as optical emission [2, 7, 11] and charged particle analysis (in preparation).

To make sure that the probes are not influencing each other, we used the probes to approximately determine the plasma parameters (via floating potential and ion saturation current) and sheath thickness [17]. We obtain a maximum plasma density of about  $2 \times 10^{16} \text{ m}^{-3}$  and a sheath thickness of about 250  $\mu\text{m}$ . Even as these parameters vary greatly, depending on time and location, we can safely assume that the probes are indeed independent from each other. Furthermore, the small sheath ensures that the probe effects are local and that plasma is not greatly affected by the presence of the probes.

## 3.2. Angular distributions

### 3.2.1 Average charge state distribution

The temporal evolution of  $I_i$  is represented on Fig. 3 for  $V_d = 550 \text{ V}$  and at a distance of 14.5 cm from the target. The anisotropy of the discharge is evident from this representation. It is also worth noting that there is no monotonous relationship between  $I_i$  and the angular position – the experiments were repeated to verify the relationship of the data points. The data suggest a non-monotonous angular dependence of the deposition rate, or the average charge state, or both. It can be expected the average charge  $\bar{Q}$  is strongly influenced by the transition to the SSS mode. Figs. 4.a and b show  $\bar{Q}$  for the discharge with 520 V and 550 V applied, with the probes positioned at 14.5 cm and 22.5 cm from the target surface, respectively. As expected,  $\bar{Q}$  is higher when the discharge includes the SSS phase, regardless of the angular position. Moreover, the transition to the metal dominated mode affects the shape of the angular distribution. It is interesting to note that, for discharges of equal parameters,  $\bar{Q}$  is always higher at 22.5 cm than at 14.5 cm. However, there is non-trivial

spatial development of the HIPIMS discharge: at 22.5 cm,  $\bar{Q}$  can be locally higher for 520 V than in the metal dominated HIPIMS mode at 550V when measured at 14.5 cm. From research on i-PVD methods in the 1990s it is known that the sputtered atoms are relatively fast and therefore more likely to be ionized after they have undergone an elastic collision with a slower atom or atom not moving away from the target. Since the mean free path is larger than the sheath thickness, ionization continues to occur relatively far from the target. The average charge state locally approaches or exceeds unity in the SSS mode in comparison to less than 0.025 for a conventional DC discharge of the same average power. This implies the presence of doubly charged Cu species in the discharge, which was linked to the secondary emission properties [14]. The spatial distributions of  $\bar{Q}$  (Fig. 5.a) and the strengths of the magnetic field (Fig. 5.b) for 14.5, 18.5 and 22.5 cm show a correlation. This can be explained by the tendency of the electrons to drift along the magnetic lines. As mentioned above, the atoms travelling from the target to the substrate have still a considerable chance to be ionized by electrons. Ions produced near the target have a high probability to return to the target due to the electric field that extends into the magnetized plasma. However, ions produced far from the target tend to follow electrons, some of them are guided away by the magnetic field lines (hence magnet balancing versus unbalancing is important). The mobility constrains of electrons perpendicular to the magnetic field lines also determine the regions of enhanced ionization probability. We should keep in mind that the main mechanism of ionization is electron impact ionization, which requires the presence of energetic electrons. Secondary electrons from the target, accelerated in the target sheath, are the main source of energetic electrons, both by themselves as well as in terms of heating the bulk electrons through electron-electron interaction. Therefore, the appearance of enhanced charge states along the regions influenced by the magnetic field should be expected.

### 3.2.2 Thickness and deposition rate distribution

The section is interesting because HIPIMS discharges are known to provide generally lower deposition rates compared to conventional magnetron discharges when normalized to the average discharge power. Here we look how the discrepancy is spatially distributed.

When the average discharge power increases from 20 W to 210 W, by increasing the discharge voltage  $V_d$  from 520 V to 550 V, the absolute deposition rate increases sharply (Figs. 6a and b). However, those HIPIMS rates are lower than the deposition rates achieved in direct current (DC) discharges with the same average power (Fig. 7a and b) regardless of the distance to target. When the HIPIMS discharge includes the SSS phase, the average deposition rates are close to 50% and 60 % of the conventional DC rates at 22.5 cm and 14.5 cm from the target, respectively.

The discrepancy is less pronounced at lower power or voltage, i.e. for  $V_d = 520$  V. Therefore, depending on the target to substrate distance, there are contrary tendencies for the average charge  $\bar{Q}$  and the deposition rate. However, it is also necessary to keep in mind a possible change in the microstructure the films, as possibly affected by the energy brought by energetic ions (as was shown for Ta films [18]). SEM cross sectional images showed that the HIPIMS films deposited at 14.5 cm are densified –even without bias– compared to the films deposited with a conventional DC discharge operated at the same pressure. All films had a columnar structure. The images were consistent with the film densities determined by the thickness and weight method: the density of HIPIMS films was about 96% of the theoretical bulk density, whereas the density of films by DC sputtering was only about 86%. One should also note that the HIPIMS copper films showed good adhesion to the silicon substrate upon fracture, while the DC films tended to delaminate.

## 4. Conclusions

The spatial distribution of copper HIPIMS discharges has been probed by monitoring the ion currents and the film thickness at different angular positions and distances from the target surface. The angular distribution of the deposition rate and the average charge state of the copper species were then deduced. For a target voltage below the threshold to the SSS phase, the deposition rate is very low and the average charge state was less than 0.4. For higher discharge voltage, when each HIPIMS pulse evolves into the SSS phase, the deposition rate is significantly higher but only approximately 50% or 60% percent of a conventional DC discharge, depending on the distance from the target. For this comparison, the rates were normalized by the average discharge power. Clearly, the advantage of HIPIMS is not in the rate but in the quality of the coating. The density of our copper coating is higher for HIPIMS than for DC sputtering when comparing the same geometrical and average power configurations. At the high voltage level, when SSS occurs, the spatial distribution of the average charge state shows similarities with the distribution of the strength of the magnetron's magnetic field. This suggests that the ionized copper species are more readily produced where energetic electrons are present and trapped, and that the plasma is drifting along the magnetic lines due to electron-ion coupling. The average charge state generally increases with the distance from the target and exhibits values that can locally exceed unity, which implies the presence of doubly charged copper ions. The angular distribution of neutrals and ions is non-trivial and depends on the parameters of the HIPIMS discharge, and in particular on whether or not the SSS phase has been reached.

### **Acknowledgments**

We gratefully thank Joe Wallig and Joakim Andersson (Berkeley Lab) and Günter Mark (Melec GmbH) for technical support. This work was supported by the Assistant Secretary for

Energy Efficiency and Renewable Energy, Office of Building Technology, of the U.S.  
Department of Energy under Contract No. DE-AC02-05CH11231.

## References

- [1] Kouznetsov V, Macak K, Schneider J M, Helmersson U, and Petrov I *Surf. Coat. Technol.* 1999 **122** 290-293.
- [2] Macak K, Kouznetsov V, Schneider J, Helmersson U, and Petrov I *J. Vac. Sci. Technol. A* 2000 **18** 1533-1537.
- [3] Ehiasarian A P, New R, Münz W-D, Hultman L, Helmersson U, and Kouznetsov V *Vacuum* 2002 **65** 147-154.
- [4] Ehiasarian A P, Hovsepian P E, Hultman L, and Helmersson U *Thin Solid Films* 2004 **457** 270-277.
- [5] Helmersson U, Lattemann M, Bohlmark J, Ehiasarian A P, and Gudmundsson J T *Thin Solid Films* 2006 **513** 1-24.
- [6] Wallin E and Helmersson U *Thin Solid Films* 2008 Available online 31 August 2007.
- [7] Bohlmark J, Alami J, Christou C, Ehiasarian A, and Helmersson U *J. Vac. Sci. Technol. A* 2005 **23** 18-22.
- [8] Bohlmark J, Lattemann M, Gudmundsson J T, Ehiasarian A P, Aranda Gonzalvo Y, Brenning N, and Helmersson U *Thin Solid Films* 2006 **515** 1522-1526.
- [9] Anders A, Andersson J, and Ehiasarian A *J. Appl. Phys.* 2007 **102** 113303-1-11.
- [10] Anders A, Andersson J, and Ehiasarian A *J. Appl. Phys.* 2008 **103** 039901-1.
- [11] Alami J, Sarakinos K, Mark G, and Wuttig M *Appl. Phys. Lett.* 2006 **89** 154104-3.
- [12] Chistyakov R, High deposition rate sputtering, Patent US 6,896,773, 2002-11-14.
- [13] Posadowski W M and Radzimski Z *J. Vac. Sci. Technol. A* 1993 **11** 2980-2984.
- [14] Anders A *Appl. Phys. Lett.* 2008 accepted for publication.
- [15] Ziegler J F and Biersack J, "Monte Carlo code SRIM2006.02, downloadable from <http://srim.org/>." 2006.

- [16] Hosokawa N, Tsukada T, and Kitahara H, “Effect of discharge current and sustained self-sputtering,” Proc. 8th Int. Vacuum Congress, Le Vide, Cannes, France, 1980, 11-14.
- [17] Anders A, *A Formulary For Plasma Physics*. Berlin: Akademie-Verlag, 1990.
- [18] Alami J, Eklund P, Andersson J M, Lattemann M, Wallin E, Bohlmark J, Persson P, and Helmersson U *Thin Solid Films* 2007 **515** 3434-3438.

### Figure captions

Figure 1 : Setup of the magnetron and probes, including a simplified electrical schematic used for this study (top), and photograph of the setup (bottom).

Figure 2 : Temporal development of the target discharge current for fixed discharge voltages of 520 V and 550 V, with a pulse duration of 400  $\mu$ s.

Figure 3 : Temporal evolution of the ion current for one discharge pulse, collected by probes placed 14.5 cm from the target, for a 550 V discharge, with the angle to the surface plane as a parameter.

Figure 4 : Angular distribution of the average charge state for probes placed at (a) 14.5 cm and (b) 22.5 cm from the target, for discharge voltages of 520 V and 550 V.

Figure 5 : (a) Angular distribution of the average charge state for probes placed at 14.5 cm, 18.5 cm, and 22.5 cm from the target with a discharge voltage of 550 V; (b) Angular distribution of the strength of the magnetron's magnetic field at 14.5 cm, 18.5 cm, and 22.5 cm from the target.

Figure 6 : Angular distributions of the HIPIMS deposition rates for 520 V and 550 V discharges measured at (a) 14.5 cm and (b) 22.5 cm.

Figure 7 : Same as figure 6 but normalized to the DC deposition rate at the same average power, measured at (a) 14.5 cm and (b) 22.5 cm.

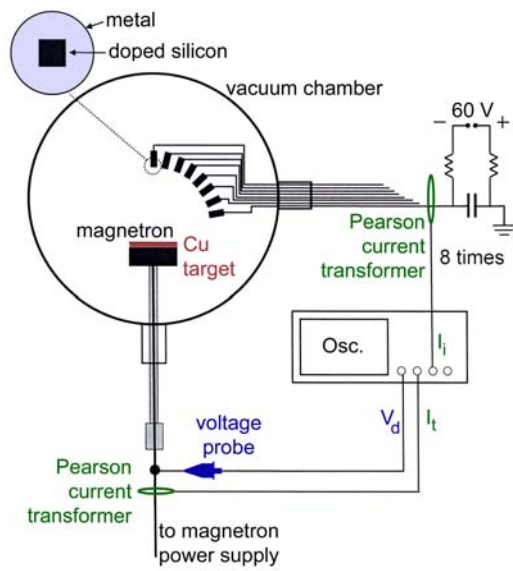


Fig. 1

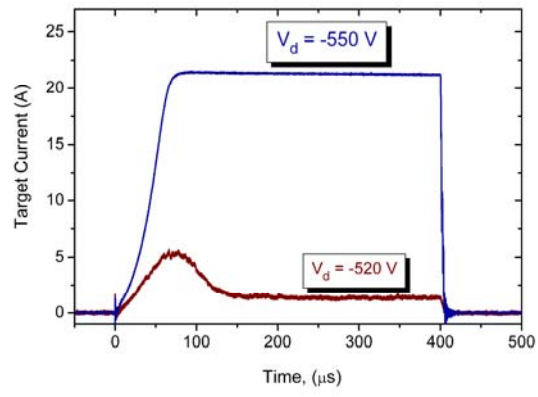


Fig. 2

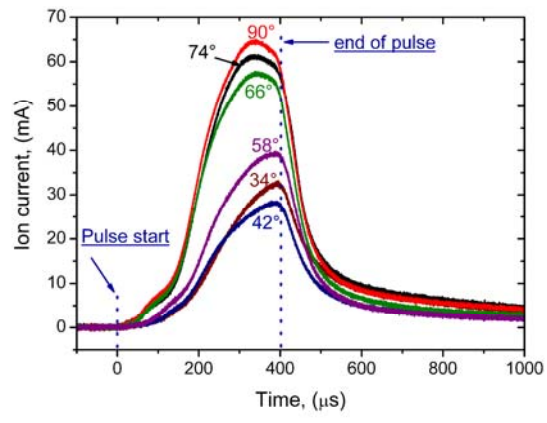


Fig. 3

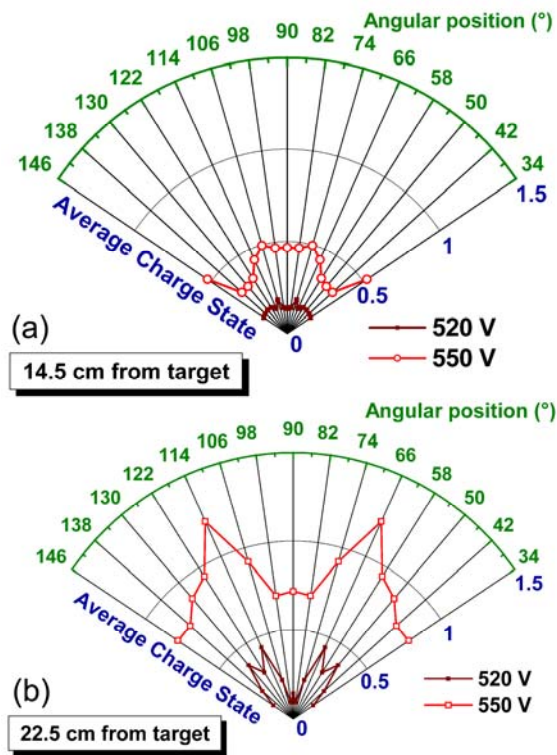


Fig. 4

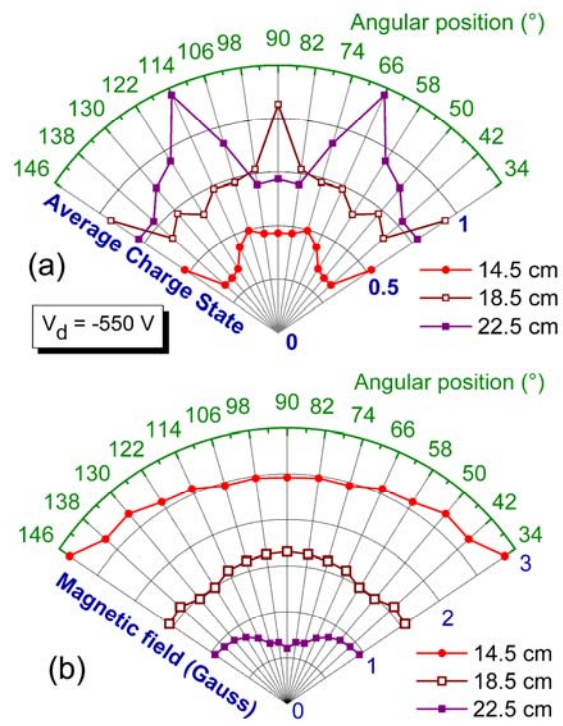


Fig. 5

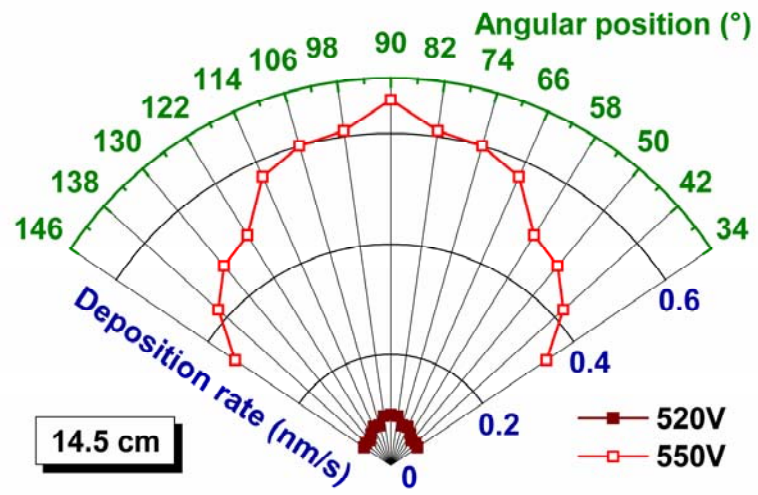


Fig. 6 a

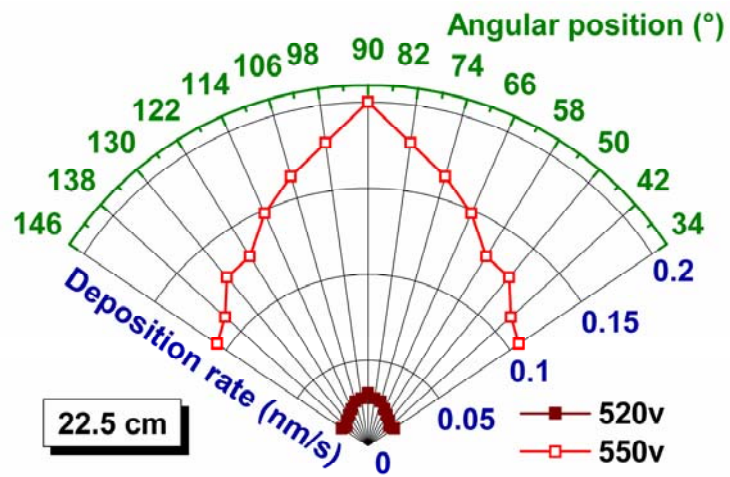


Fig. 6 b

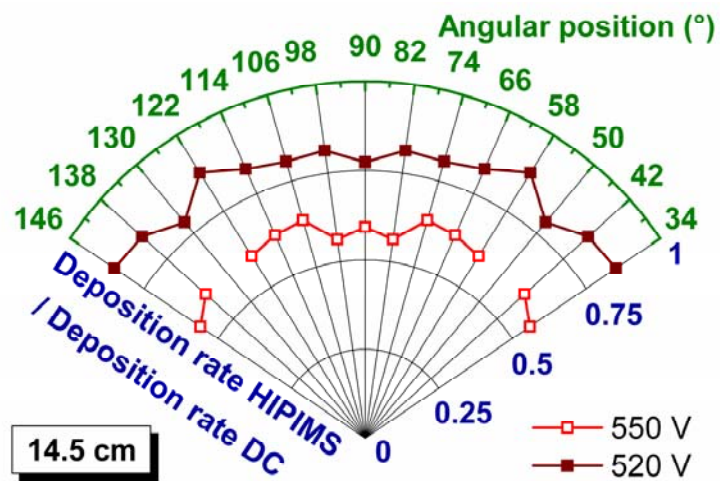


Fig. 7 a

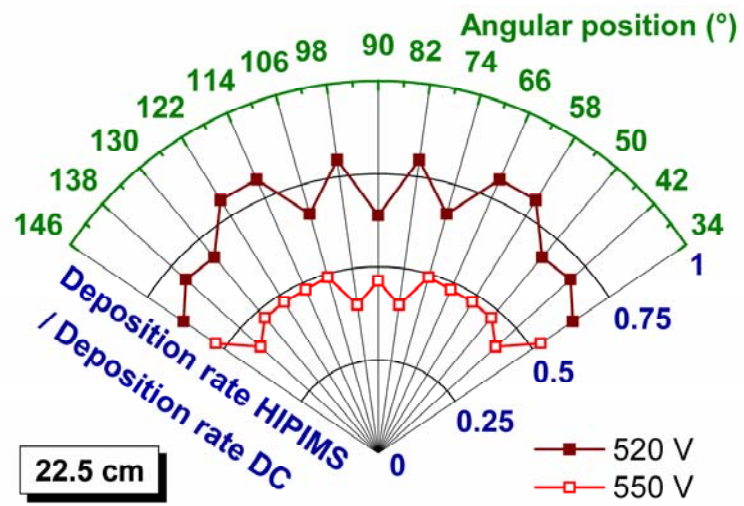


Fig. 7 b